Suppression of the rate of growth of dynamic heterogeneities and its relation to the local structure in a supercooled polydisperse liquid

Sneha Elizabeth Abraham and Biman Bagchi*
Solid State and Structural Chemistry Unit, Indian Institute of Science, Bangalore 560 012, India
(Received 24 July 2008; published 3 November 2008)

The relationship between the microscopic arrangement of molecules in a supercooled liquid and its slow dynamics at low temperature near glass transition is studied by molecular dynamics simulations. A Lennard-Jones liquid with polydispersity in size and mass of constituent particles is chosen as the model system. Our studies reveal that the local structure (that varies with polydispersity) plays a crucial role both in the slowing down of dynamics and in the growth of the dynamic heterogeneities, besides determining the glass forming ability of the system. Increasing polydispersity at fixed volume fraction is found to suppress the rate of growth of dynamic correlations, as detected by the growth in the peak of the nonlinear density response function, $\chi_4(t)$. The growth in dynamical correlation is manifested in a stronger than usual breakdown of Stokes-Einstein relation at lower polydispersity at low temperatures and also leads to a decrease in the fragility of the system with polydispersity. We show that the suppression of the rate of growth of the dynamic heterogeneity can be attributed to the loss of structural correlations (as measured by the structure factor and the local bond orientational order) with polydispersity. While a critical polydispersity is required to avoid crystallization, we find that a further increase in polydispersity lowers the glass forming ability.

DOI: 10.1103/PhysRevE.78.051501 PACS number(s): 64.70.pm, 61.20.Lc, 82.70.Dd

I. INTRODUCTION

The relation between the local structure and its slow dynamics in a supercooled liquid near glass transition temperature, T_g, is currently a subject of intense curiosity. The most distinctive feature of glass formation is the rapid increase of viscosity with a decrease in temperature. The temperature at which the viscosity becomes 10^{13} Poise is defined as the glass transition temperature. One of the main difficulties in understanding the glass transition phenomenon is that this enormous slowing down of dynamics is apparently not accompanied by a growing static correlation length (unlike the usual critical phenomena). Static structural quantities do not reveal any long-range correlation. In fact, the static structure of the liquid near glass transition is not much different from its equilibrium high-temperature counterpart.

In the Adam-Gibbs picture [1], the sharp slowing down is related to the growth of a cooperative dynamic length scale. In a separate theoretical study, the size of heterogeneous reconfiguring regions in a viscous liquid was inferred via the random first-order transition theory (RFOT) [2]. There is now increasing evidence from both experiments and simulations of a dynamic correlation length that grows upon approaching the glass transition [3–5]. Multipoint susceptibilities have been devised to quantify the behavior and magnitude of growing dynamic length scales and have been used in the experimental studies for several materials [4]. These have directly determined the number of molecular units that move cooperatively near glass transition. The simplest density correlation function that contains information on correlated motion is the fourth order [6,7]. The four-point time-dependent density correlation function $g_4(r,t)$ measures the spatial correlations between the local liquid density at two points in space, each at two different times. The dynamical four-point susceptibility, $\chi_4(t)$ [the volume integral of $g_4(r,t)$], becomes increasingly pronounced as glass transition is approached.

In this study, we look for a possible relationship between the structure and the slowdown of dynamics in supercooled polydisperse liquids near glass transition. In particular, we look at how the local structure (which we characterize using structure factor and bond orientational order parameters) would influence the growth of dynamic heterogeneity and the glass forming ability of the system. Polydisperse liquids are one of the simplest model systems that exhibit glass transition and can be conveniently studied via both experiments [8,9] and computer simulations [10,11] as the size distribution of particles prevents crystallization. It also serves as a model for colloids and many other real world systems such as polymers, pigments, paints, etc., as polydispersity is inherent in all these systems. Polydispersity introduces a distribution of particle diameters and masses and thus makes the system intrinsically more heterogeneous. However, the effect of polydispersity on dynamic heterogeneity has not yet been examined in detail. Here we probe this in detail using the dynamical four-point susceptibility, $\chi_4(t)$. Increasing polydispersity results in the loss of structural order. Thus by varying polydispersity, one can understand the effect of loss of structure on the growth of dynamic heterogeneities. Our studies [11] have shown that increasing polydispersity at fixed volume fraction decreases the fragility, hence this study also presents us with an opportunity to probe the growth of four-point susceptibility (and thus dynamic heterogeneity) in systems with varying degrees of fragility.

The rest of the paper is organized as follows. In Sec. II, we describe the model and simulation details and also define various quantities that are used in the analysis. In Sec. III, we present our results and give detailed discussions on the same. We give our concluding remarks in Sec. IV.

*bbagchi@sscu.iisc.ernet.in

II. THEORY AND COMPUTATIONAL METHODS

A. Four-point susceptibility

The two-point, two-time, fourth-order density correlation function [6,7,12] is defined as

$$g_4(\vec{r}_1,\vec{r}_2,t) \equiv \langle \rho(\vec{r}_1,0)\rho(\vec{r}_1,t)\rho(\vec{r}_2,0)\rho(\vec{r}_2,t)\rangle - \langle \rho(\vec{r}_1,0)\rho(\vec{r}_1,t)\rangle \times \langle \rho(\vec{r}_2,0)\rho(\vec{r}_2,t)\rangle. \quad (1)$$

The volume integral of $g_4(r_1,r_2,t)$ gives the four-point susceptibility $\chi_4(t)$,

$$\chi_4(t) = \frac{\beta V}{N^2} \int\int d\vec{r}_1 d\vec{r}_2 \rho(\vec{r}_1,0)\rho(\vec{r}_2,t) g_4(\vec{r}_1,\vec{r}_2,t). \quad (2)$$

It has been shown that $\chi_4(t)$ can be written as [7]

$$\chi_4(t) = \frac{\beta V}{N^2}[\langle Q^2(t)\rangle - \langle Q(t)\rangle^2]. \quad (3)$$

Here $\beta = \frac{1}{k_B T}$ and $Q(t)$ is a time-dependent order parameter and is given by

$$Q(t) = \int\int d\vec{r}_1 d\vec{r}_2 \rho(\vec{r}_1,0)\rho(\vec{r}_2,t) w(|\vec{r}_1 - \vec{r}_2|) = \sum_{i=1}^{N}\sum_{j=1}^{N} d\vec{r} w(|\vec{r}_1 - \vec{r}_2|)\,\delta(\vec{r} + \vec{r}_i(0) - \vec{r}_j(t)). \quad (4)$$

$w(r)$ is the overlap function that is unity inside a region of size a and zero otherwise, where a is taken on the order of particle diameter. In our studies, we choose $a=0.40$ for all the systems with different polydispersity. $Q(t)$ measures the number of particles that in a time t has either remained within a distance a of their original position (when $i=j$) or were replaced by another particle (when $i \neq j$). We can separate Q into self- and distinct parts, $Q(t)=Q_S(t)+Q_D(t)$. The self-part corresponds to terms with $i=j$, $Q_s(t)=\Sigma w[|r_i(0) - r_j(t)|]$. The distinct part is given by $Q_D(t)=\Sigma\Sigma_{i\neq j} w[|r_i(0) - r_j(t)|]$. The susceptibility $\chi_4(t)$ can then be decomposed into self-, distinct, and cross terms [7],

$$\chi_4(t) = \chi_4^S(t) + \chi_4^D(t) + \chi_4^{SD}(t), \quad (5)$$

where,

$$\chi_4^S(t) \propto \langle Q_S^2(t)\rangle - \langle Q_S(t)\rangle^2, \quad (6)$$

$$\chi_4^D(t) \propto \langle Q_D^2(t)\rangle - \langle Q_D(t)\rangle^2, \quad (7)$$

and

$$\chi_4^{SD}(t) \propto \langle Q_S(t)Q_D(t)\rangle - \langle Q_S(t)\rangle\langle Q_D(t)\rangle. \quad (8)$$

As has been found in previous studies [7], we find that for our model system also the major contribution to $\chi_4(t)$ comes from $\chi_4^S(t)$, hence in this paper we have presented results only for $\chi_4^S(t)$.

B. Bond-orientational order

The average microscopic structure of liquids is usually described by the radial distribution function or the structure factor, which essentially measures only the density-density correlation function. However, bond-orientational order parameters (BOP) introduced by Steinhardt *et al.* [13–15] give a better quantification of the local structure as they capture the symmetry of bond orientations. BOP are described in terms of combinations of spherical harmonic functions. Consider a system of N particles. First, one defines a set of "bonds" which are defined as the vectors connecting neighboring particles. All particles j within a cutoff distance r_0 of particle i are defined as neighbors of particle i. Here r_0 is chosen to be equal to the distance to the first minimum of the radial distribution function (RDF). The local order parameters associated with a bond r are the set of numbers

$$Q_{lm}(r) \equiv Y_{lm}(\theta(r),\phi(r)), \quad (9)$$

where $\theta(r)$ and $\varphi(r)$ are the polar and azimuthal angles of the bond with respect to an arbitrary but fixed reference frame, and $Y_{lm}(\theta(r),\varphi(r))$ are the spherical harmonic functions. It is useful to consider only the even-l spherical harmonics, which are invariant under inversion. Global bond-order parameters can be calculated by averaging over all the bonds in the system,

$$\bar{Q}_{lm} \equiv \frac{1}{N_b}\sum_{\text{bonds}} Q_{lm}(\vec{r}). \quad (10)$$

Since Q_{lm}'s for a given l depend on the rotations of the reference frame, it is important to consider the rotationally invariant combinations such as

$$Q_l \equiv \left(\frac{4\pi}{2l+1}\sum_{-l}^{l} |\bar{Q}_{lm}|^2\right)^{1/2} \quad (11)$$

and

$$W_l \equiv \sum_{m_1,m_2,m_3}^{m_1+m_2+m_3=0} (\cdots)\bar{Q}_{lm_1}\bar{Q}_{lm_2}\bar{Q}_{lm_3}. \quad (12)$$

Q_l and W_l are the second- and third-order invariants, respectively. The coefficients $(\cdots)$ are Wigner $3j$ symbols. One also defines a normalized quantity,

$$\hat{W}_l \equiv \frac{W_l}{\left(\sum_m |Q_{lm}|^2\right)^{3/2}}, \quad (13)$$

which for a given l is independent of the magnitudes of the Q_{lm}. The four bond-order parameters Q_4, Q_6, $\hat{W}_4$, and $\hat{W}_6$ are sufficient to identify different crystal structures. The typical values of these for different crystal structures are given in [15]. For a liquid, the global values of all these four quantities are zero as there is no long-range order. Note that in clusters with cubic symmetry, nonzero averages occur only for $l \geqslant 4$ whereas nonzero averages occur only at $l=6$ and 10 for icosahedral cluster.

C. System and simulation details

Microcanonical (NVE) ensemble molecular dynamics (MD) simulations are carried out in three dimensions on a

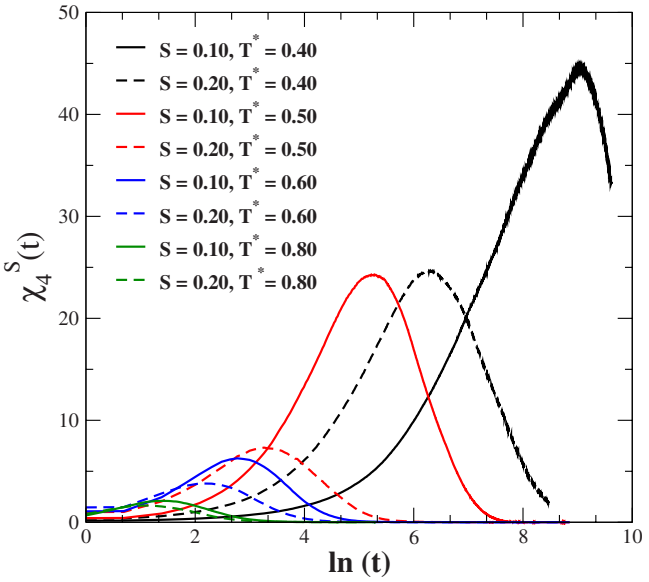

FIG. 1. (Color online) The time dependence of the four-point susceptibility $[\chi_4^S(t)]$ at four different temperatures and at two different polydispersity, $S=0.10$ (thick lines) and $S=0.20$ (dashed lines). From the bottom to the top, temperature decreases. $\chi_4^S(t)$ grows for both systems as T decreases, but there is a more pronounced growth at lower polydispersity.

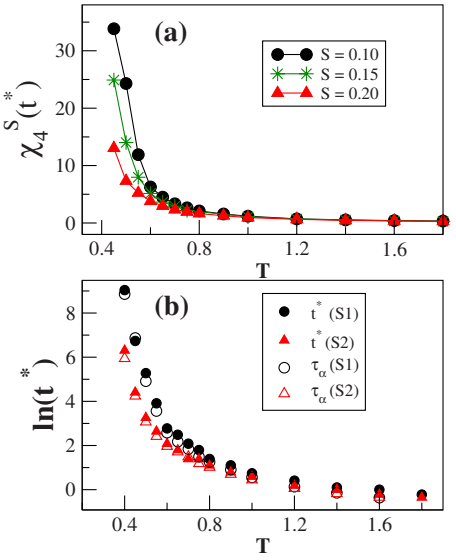

FIG. 2. (Color online) (a) The value of the peak height of $\chi_4^S(t)$ is plotted as a function of T for $S=0.10$ (filled circle), $S=0.15$ (star), and $S=0.20$ (filled triangle) systems. The figure shows the suppression of the rate of growth of dynamic heterogeneity with S. (b) The time at which $\chi_4^S(t)$ peaks, t^*, is plotted as a function of T for $S=0.10$ (S1) and $S=0.20$ (S2) systems (filled circles and triangles, respectively). t^* is similar to the α-relaxation time (open circles and triangles, respectively). The latter is obtained by doing KWW fit to $F_s(k_{\max},t)$ where $k_{\max}$ corresponds to the first peak in the static structure factor.

system of $N=864$ particles of mean diameter $\bar{\sigma}$ with polydispersity in both size and mass. The polydispersity in size is introduced by random sampling from the Gaussian distribution of particle diameters σ,

$$P(\sigma) = \frac{1}{\sqrt{2\pi}\delta} \exp\left[-\frac{1}{2}\left(\frac{\sigma-\bar{\sigma}}{\delta}\right)^2\right]. \tag{14}$$

The standard deviation δ of the distribution divided by its mean $\bar{\sigma}$ gives a dimensionless parameter, the polydispersity index $S=\frac{\delta}{\bar{\sigma}}$. The mass m_i of particle i is scaled by its diameter $m_i=\bar{m}(\frac{\sigma_i}{\bar{\sigma}})^3$. We have chosen $\bar{m}=1.0$. The simulations are carried out at different values of the polydispersity index, S, but at fixed volume fraction, $\varphi=0.52$. The interactions between the particles are given by the shifted-force Lennard-Jones (LJ) 12-6 potential,

$$U_{ij} = 4\epsilon_{ij}\left[\left(\frac{\sigma_{ij}}{r_{ij}}\right)^{12} - \left(\frac{\sigma_{ij}}{r_{ij}}\right)^{6}\right], \tag{15}$$

where i and j represent any two particles and $\sigma_{ij}=(\frac{\sigma_i+\sigma_j}{2})$. The LJ interaction parameter ϵ_{ij} is assumed to be the same for all particle pairs and set equal to unity. The particles are enclosed in a cubic box and periodic boundary conditions are used. The cutoff radius r_c is chosen to be $2.5\bar{\sigma}$. A time step of 0.001 is employed for $T\geqslant 1.0$ and 0.002 for $T<1.0$. All quantities in this study are given in reduced units [length in units of σ, temperature in units of $\frac{\epsilon}{k_B}$, and time in units of $\tau=(\frac{\bar{m}\bar{\sigma}^2}{\epsilon})^{1/2}$].

III. RESULTS AND DISCUSSION

The main objective of our study is to demonstrate the effect of polydispersity and hence of the local structure on the growth of dynamic heterogeneities. By varying polydispersity, we can "tune" the local structure and hence study its effects on the dynamic heterogeneity. As polydispersity is increased, the local structure is progressively destroyed. Hence the blocking of the particles in the cages of the neighboring particles (as required for the mode-coupling theory of dynamic transition [17]) becomes ineffective at higher polydispersity. We find that this has a pronounced effect on the development of dynamic heterogeneities as well. In this section, we systemically present our results and show that the local structure plays a very important role in determining the dynamics in supercooled liquids near glass transition.

A. Suppression of the rate of growth of dynamic correlations by polydispersity

The four-point susceptibility $\chi_4^S(t)$ obtained from Eq. (3) is shown in Fig. 1 for $S=0.10$ and 0.20 for a few temperatures. From Eqs. (1) and (2), we see that $\chi_4(t)$ becomes larger when the dynamic fluctuations become increasingly spatially correlated. Since $\chi_4(t)$ is the volume integral of the four-point correlator $g_4(r,t)$, it is directly related to the number of correlated particles. As temperature is lowered, $\chi_4^S(t)$ grows for both systems but the rate of growth decreases with polydispersity. This is more clearly seen in Fig. 2(a), where the peak height of $\chi_4^S(t)$ [which we label as $\chi_4^S(t^*)$] is plotted

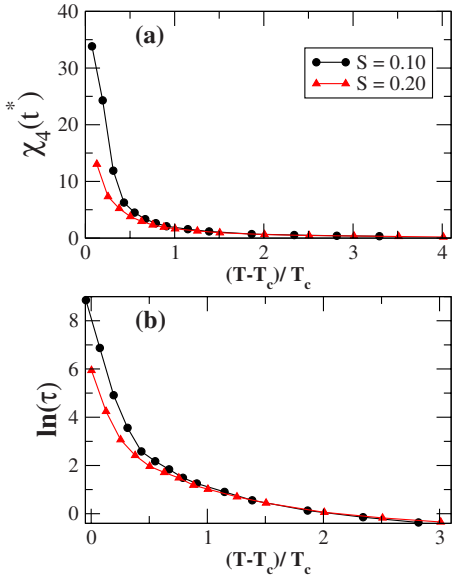

FIG. 3. (Color online) (a) $\chi_4^S(t^*)$ as a function of the distance from the MCT critical temperature T_c for $S=0.10$ and 0.20 systems. T_c values are 0.42 and 0.39 for $S=0.10$ and 0.20 systems, respectively. (b) α-relaxation time, τ_α, as a function of the distance from T_c.

against temperature for different values of polydispersity. Figure 2(a) shows the suppression of the rate of growth of dynamical heterogeneity by polydispersity. In Fig. 3(a), we plot the peak height $\chi_4^S(t^*)$ as a function of the distance from the mode-coupling theory (MCT) critical temperature T_c for the $S=0.10$ and 0.20 systems. The rescaled plot also shows a suppression in the rate of growth of $\chi_4^S(t^*)$ for the $S=0.20$ system as compared to the $S=0.10$ system. By fitting to the expression $\chi_4(t^*) \sim (\frac{T-T_c}{T_c})^{\gamma_\chi}$, we get the values of the exponent γ_χ as 1.507 and 1.188 for $S=0.10$ and 0.20 systems, respectively. The exponent γ_χ thus seems to change with polydispersity. The suppression of the rate of growth of dynamical heterogeneity by polydispersity leads to the dynamic crossovers observed in the values of the stretch exponent, β, and the non-Gaussian parameter, $\alpha_2(t)$, between $S=0.10$ and 0.20 systems as shown earlier [11] and the crossover behavior seen in the exponent z_σ that quantifies the deviation from the prediction of the Stokes-Einstein relation (see Sec. III B). Increasing polydispersity at fixed volume fraction decreases the fragility of the system (see Fig. 4). Fragility measures the rapidity with which the system approaches glass transition. Hence a decrease in the rate of growth of dynamic heterogeneity with polydispersity is consistent with the decrease in the fragility. This is further explained in Sec. III C.

In Fig. 2(b), we show the time at which $\chi_4^S(t)$ peaks, t^*, versus temperature for $S=0.10$ and 0.20. Also shown are the α-relaxation times, τ_α, obtained by doing a Kohlrausch-William-Watts (KWW) fit to the self-part of intermediate scattering function, $F_s(k,t)$. The plot shows that the dynamics is maximally correlated on time scales of the order of the α-relaxation time. In Fig. 3(b), τ_α is plotted as a function of the distance from the MCT critical temperature, T_c. The rescaled plot shows that the rate of growth of τ_α decreases with polydispersity.

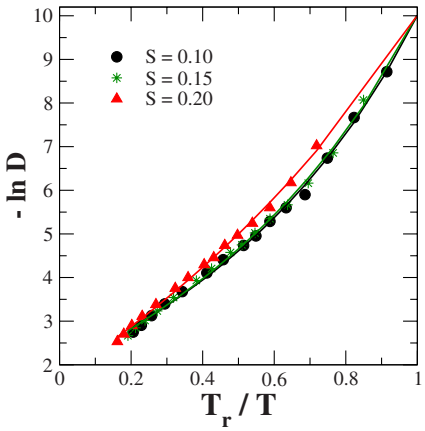

FIG. 4. (Color online) Angell-like fragility plot at different S. The thick lines are VFT fit to the diffusivity data, $D = D_0 \exp(\frac{E_D}{T-T_0})$. The reference temperature T_r is chosen such that $D(T_r)=4.5\times10^{-5}$. The VFT extrapolation is used to locate T_r. The plot shows that fragility decreases with S. Strength parameter m (where $m=\frac{E_D}{T_0}$ [16]) obtained from VFT fit has the values 7.78, 8.54, and 15.94 for $S=0.10$, 0.15, and 0.20 systems, respectively.

B. Breakdown of Stokes-Einstein relation

In this section, we discuss the breakdown of the Stokes-Einstein (SE) relation and its connection to the rate of growth of dynamic heterogeneity in the system as temperature is lowered. The SE relation is based on treating the liquid as a continuum, and is given by

$$D = \frac{k_B T}{C \eta \sigma}. \tag{16}$$

Here C is a constant that depends on the boundary conditions (stick or slip) and η is the viscosity. If the Stokes-Einstein relation is strictly valid, then a plot of $\ln(D_i/D_j)$ versus $\ln(\sigma_j/\sigma_i)$ would be a straight line with unit slope. Here i and j are indices for solute and solvent, respectively. In Fig. 5, we show this plot for the $S=0.10$ and 0.20 systems. Both systems show deviation from the SE prediction even at high temperatures due to the intrinsic heterogeneity in the system, with the deviation being more pronounced for the $S=0.20$ system. The SE relation has been shown not to be valid for the diffusion of small solutes in a solvent of bigger particles [18]. There is an anomalous enhancement of the self-diffusion over the SE value for small solutes that can be described by a power law,

$$\frac{D_i}{D_j} \sim \left(\frac{\sigma_j}{\sigma_i}\right)^{z_\sigma}. \tag{17}$$

Hence the exponent z_σ quantifies the deviation from the SE relation. It is unity in the SE limit and usually larger than unity in supercooled liquid. Figure 6 shows that z_σ deviates significantly from unity for polydisperse liquids, particularly at low temperatures. Interestingly, it is larger than unity even at high temperature because of the heterogeneity in the size and mass. This deviation of the slope from unity at high temperature can be a combination of two different effects. The first one is the mass, which is not present in the SE

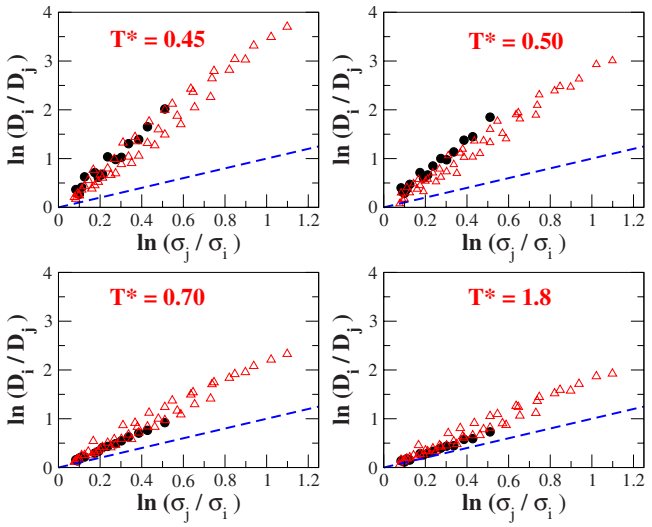

FIG. 5. (Color online) The plot of $\ln(D_i/D_j)$ versus $\ln(\sigma_j/\sigma_i)$ for $S=0.10$ (circles) and $S=0.20$ (triangles). Here the subscript i denotes the smaller particle. If the SE relation is valid, this plot would be of unit slope (dashed line). The plot shows that at high temperature, the deviation from the Stokes-Einstein prediction is higher for the $S=0.20$ system, but the scenario reverses at low temperature where the $S=0.10$ system shows a stronger deviation due to the faster growth of dynamic heterogeneity.

relation but has been reported earlier in simulations [19] and MCT studies [20]. The studies predict a weak power-law mass dependence of diffusion. The second effect is that of size, which has also been obtained in experiments and simulations [21] and MCT studies [18]. When the size of one of the particles is 1.5–15 times smaller than the other, it shows an anomalous rise in diffusion. This enhanced diffusion has been explained in terms of the microviscosity effect. The MCT studies explain the microscopic origin of the size effect

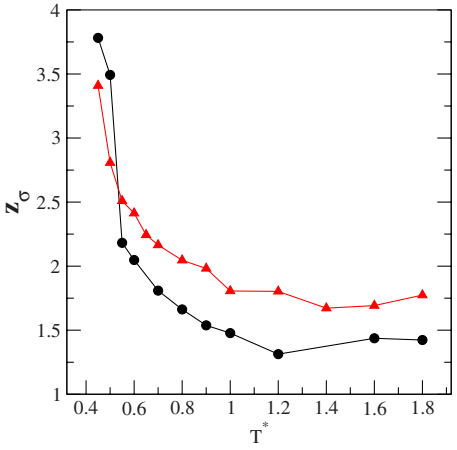

FIG. 6. (Color online) The values of the power-law exponent, z_σ, obtained by fitting Eq. (17), are plotted against T for $S=0.10$ and 0.20 systems. If the SE relation is strictly valid, then $z_\sigma=1$. Deviation from unity shows the breakdown of SE relation. The figure clearly shows that at high temperatures, intrinsic heterogeneity causes a larger breakdown in the $S=0.20$ system, whereas at low temperatures the faster growth of dynamic heterogeneity leads to a stronger breakdown in the $S=0.10$ system.

in terms of the difference in relaxation time scales of the two particles, which leads to a decoupling in the dynamics [18]. (Note that for size-dependent studies, the small particle was a tracer and for mass-dependent studies the heavier particle was a tracer. In the present study, the systems are intrinsically heterogeneous.)

As temperature is lowered, the deviation from the prediction of the SE relation becomes more pronounced and one observes a crossover in the value of z_σ between the $S=0.10$ and 0.20 systems; the values are much higher for the $S=0.10$ system than the $S=0.20$ system at low temperatures (see Fig. 6). This again shows that the rate of growth of dynamic heterogeneity is faster in the $S=0.10$ system than in the $S=0.20$ system. The faster rate of growth of dynamic correlations leads to similar temperature-dependent crossovers between the $S=0.10$ and 0.20 systems in the values of the stretch exponent (β) and the non-Gaussian parameter [$\alpha_2(t)$], both of which contain implicit information on dynamic heterogeneity [11]. These studies show that there is a strong correlation between the growing dynamic heterogeneity in the system and the breakdown of the SE relation as the former renders the continuum description of liquid invalid as required for the SE relation.

C. Fragility and the growth of dynamic correlations

It has been shown that the dynamics of fragile liquids is more spatially heterogeneous than that of strong liquids [22]. Increasing polydispersity at fixed volume fraction decreases the fragility of the system, as shown in Fig. 4. The decrease of the rate of growth of $\chi_4(t)$ with polydispersity supports the previously observed correlation between fragility and dynamic heterogeneity. The intrinsic heterogeneity of the system (as measured by the distribution of particle masses and sizes) increases with polydispersity. Hence we have the interesting scenario in which increasing polydispersity leads to a more *homogeneous* dynamics even though the system becomes completely amorphous at higher values of polydispersity. It has been shown that polydispersity has a pronounced effect on potential energy surface [23]. As polydispersity is increased from zero, the characteristics of the potential energy minima change from that of crystalline to that of amorphous. The latter is known to have low curvature and small barriers along some coordinates [24,25]. This observation is also consistent from the perspective of the inherent structure formalism, according to which the potential energy landscape of a fragile liquid is very heterogeneous, which in turn leads to heterogeneous dynamics, whereas the landscape of strong liquids consist of a single megabasin [26]. Hence from a potential energy landscape perspective, increasing polydispersity leads to a *smoothening* of the landscape that in turn leads to the facilitation of dynamics as well as a decrease of fragility. In Sec. III D, we try to understand how polydispersity suppresses the rate of growth of dynamic correlations, and in particular whether the loss of structure upon increasing polydispersity has any role to play in this.

D. Local structure and the growth of dynamic heterogeneities

We plot the static structure factor, $S(k)$, for $S=0.10$ and 0.20 systems in Fig. 7. The plot shows that increasing poly-

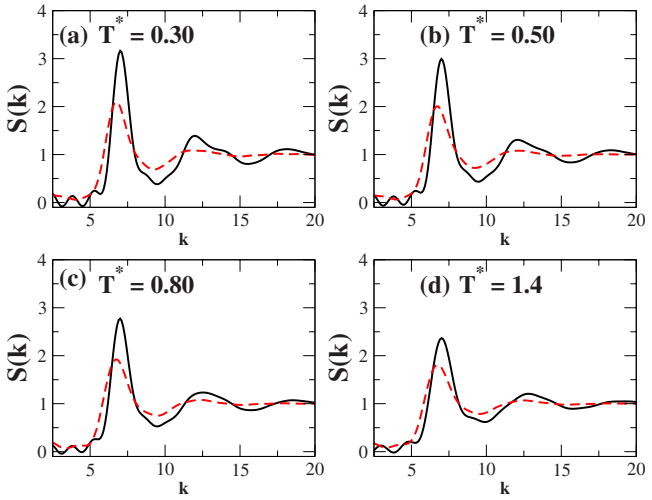

FIG. 7. (Color online) The calculated static structure factor, $S(k)$, is plotted against wave number k for $S=0.10$ (thick lines) and $S=0.20$ (dashed lines) systems at a few temperatures. Structural correlation is weaker in the $S=0.20$ system than in the $S=0.10$ system and shows no appreciable change with temperature.

dispersity destroys the local structure in the system as the system becomes more amorphous. The peak height of $S(k)$ is highly suppressed in the $S=0.20$ system as compared to the $S=0.10$ system and does not show any appreciable growth upon lowering of T. Figure 8 shows the peak height value of RDF, $g(r_{\max})$, as a function of temperature. At $S=0.10$, the peak height shows considerable enhancement upon lowering of temperature, whereas at $S=0.20$ there is no remarkable change in the value of $g(r_{\max})$ with temperature.

As mentioned in Sec. II B, the bond orientational order parameters give a better quantification of the local structural

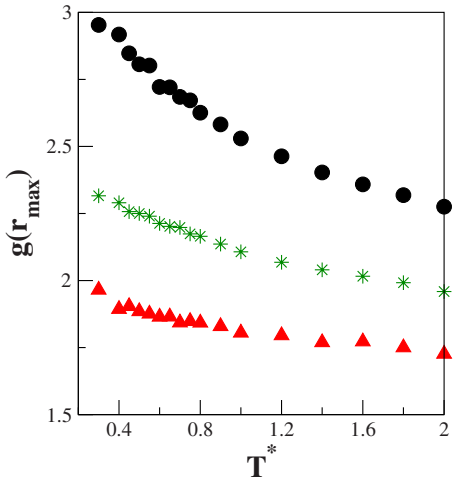

FIG. 8. (Color online) Peak height value of the radial distribution function, $g(r_{\max})$, when plotted against separation r, is plotted as a function of T for $S=0.10$ (circles), $S=0.15$ (stars), and $S=0.20$ (triangles). The $S=0.20$ system does not show any remarkable change in the value of $g(r_{\max})$ upon lowering of T. On the other hand, the $S=0.10$ system shows a sudden increase of spatial correlations for $T \leqslant 0.8$. Comparison between Figs. 8 and 2(a) shows that local structure plays a crucial role in the buildup of dynamic correlations.

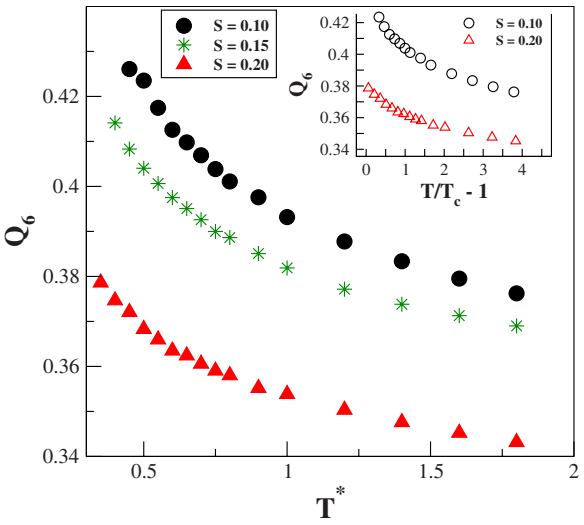

FIG. 9. (Color online) The calculated local values of bond-order parameter, Q_6, are plotted as a function of T for $S=0.10$ (circles), $S=0.15$ (stars), and $S=0.20$ (triangles). The plot shows that at the local level, there is significant orientational order that increases with a decrease in temperature and decreases with polydispersity. (Inset: Q_6 as a function of the distance from T_c.)

arrangement. Frank [27] proposed that atoms might form icosahedral clusters in liquids since the lowest-energy state of a 13-atom cluster interacting via Lennard-Jones potential is an icosahedron (and not fcc). But icosahedra cannot tile space in three-dimensions due to its fivefold symmetry and hence do not satisfy the global structural stability criterion. This geometrical frustration could be an important factor that contributes to the stability of a glassy state [28]. Steinhardt *et al.* [13] have shown that there is a long-range orientational icosahedral order in supercooled liquids. It has been shown that the large size disparities at higher values of polydispersity would inhibit any icosahedral cluster formation. However, since at low or moderate polydispersity the peak height of $g(r_{\max})$ shows a pronounced growth as temperature is lowered, one can ask whether this is due to the formation of icosahedral clusters that grow with a decrease in temperature.

We look for the local values of BOP in order to understand whether local orientational order plays any role in the growth of dynamic heterogeneities. The icosahedral order, if present, would be picked by the BOP corresponding to $l=6$, Q_6. The local values of Q_6 are plotted in Fig. 9. To get the local values, the spherical harmonics corresponding to $l=6$ are summed over the nearest-neighbor bonds only. The figure shows that there is a pronounced icosahedral orientational order at the local level. This local icosahedral order shows considerable enhancement at lower polydispersity as temperature is lowered (for $T \leqslant 0.80$) and also decreases with polydispersity. In the inset of Fig. 9, we plot Q_6 as a function of the distance from the MCT critical temperature T_c, which shows that as temperature is lowered, Q_6 increases much more sharply at lower values of S.

In Fig. 10, we plot the global values of Q_6 for different S as a function of temperature. The averages over bonds are evaluated by summing over all bonds lying within a sphere

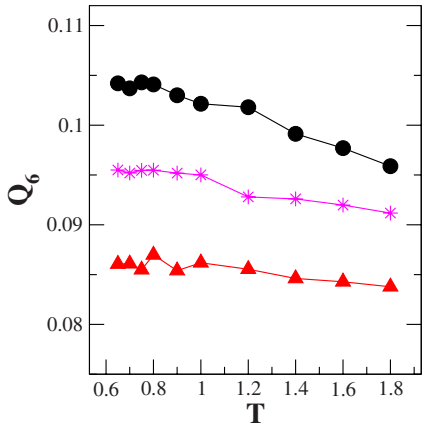

FIG. 10. (Color online) The calculated values of the global bond-order parameter, Q_6, are plotted as a function of T for $S=0.10$ (circles), $S=0.15$ (stars), and $S=0.20$ (triangles). The plot shows that there is no appreciable long-range orientational order developing in the supercooled state.

of radius 2.4 units. Nine such spheres are considered whose centers lie at different locations of the simulation box. We repeat this averaging for several different snapshots obtained from simulation. It is evident from Fig. 10 that polydispersity suppresses long-range orientational order. Even at moderate polydispersity, there is no pronounced growth of long-range icosahedral order upon supercooling.

Our results indicate that increasing polydispersity destroys both the local structure and the local orientational order. The four-point susceptibility $\chi_4^S(t)$ measures the susceptibility arising from the number of localized particles and is a measure of the dynamic heterogeneity in the system. Thus the dynamic heterogeneity is associated with the temporary localization of particles by their neighbors. Since the local structure is destroyed, at higher values of polydispersity it is not possible to have such a caging effect. As a consequence, particle motion gets decorrelated over much shorter time scales. This is best seen by plotting the van Hove correlation function (see Figs. 11 and 12). Thus the loss of local structure due to polydispersity suppresses the growth of dynamic heterogeneity in the system.

E. Polydispersity and glass forming ability

We find that the present system of LJ particles of varying size and mass crystallizes when polydispersity is less than 7.5%. Thus, our system with 10% polydispersity can be regarded as the system on the lower side of polydispersity that could be made to avoid crystallization and remain liquid within our MD simulation time range. Interestingly, we find that this is also the system that shows glassy behavior at the highest temperature. When we increase polydispersity beyond 10%, we need to lower the temperature to capture the onset of slow glassy dynamics. This can be seen from Fig. 2(b), which shows that the rate of growth of τ_α decreases with S. The new aspect revealed in the present work is the correlation between the glass forming ability (GFA) and the rate of growth of the dynamic heterogeneity—the sharper the growth, the larger the GFA.

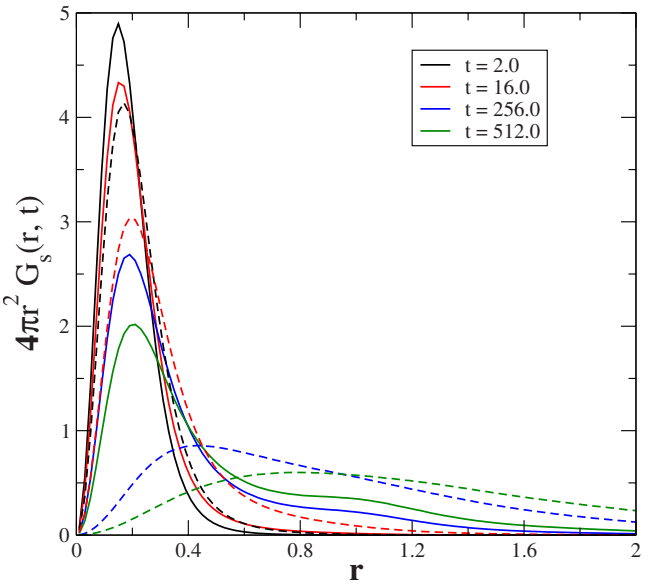

FIG. 11. (Color online) The calculated van Hove self-correlation function, $G_s(r,t)$, plotted against position r at different times (indicated in the figure) for $S=0.10$ (thick lines) and $S=0.20$ (dashed lines) systems at $T=0.45$. The figure shows the faster decay of density correlations for the $S=0.20$ system as compared to the $S=0.10$ system.

Given that a polydisperse liquid with low polydispersity ($S<0.05$) crystallizes easily, the loss of local structure at large S ($\geqslant 0.20$) and the concomitant difficulty of glass formation at large S imply a rather narrow range of S for polydisperse systems to act as good glass formers. This means that only at moderate polydispersity does the system have a high GFA. The GFA decreases with polydispersity beyond a

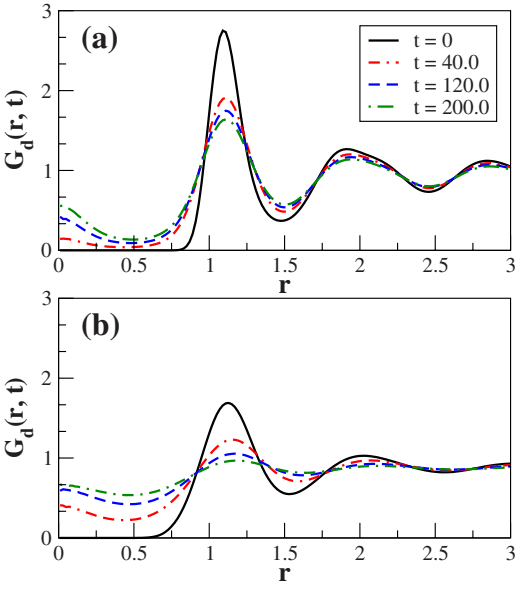

FIG. 12. (Color online) The calculated van Hove distinct-correlation function, $G_d(r,t)$, is plotted against position r for $S=0.10$ (upper panel) and $S=0.20$ (lower panel) systems at $T=0.45$ depicting the faster decay of interparticle correlations at higher polydispersity.

value of S. Further insight can be gained from the study of inherent structures. We find that the ruggedness of potential energy landscape decreases with S, which is consistent with a decrease of the GFA as well as fragility with S. It is important to note that network glass formers such as silica, which is a strong liquid in Angells fragile/strong classification, exhibits high glass forming ability due to trapping by defects. This apparently contradicts the decrease of GFA with polydispersity. The latter appears to be a hallmark of polydisperse systems. We shall address these issues in detail elsewhere.

IV. CONCLUDING REMARKS

The hypothesis that *structure determines dynamics* has been termed by Harowell as the *central dogma of glass science* [29]. This dogma is validated in the mode-coupling theory. The Adams-Gibbs theory, however, gives greater emphasis on the emergence of a dynamical correlation length as the source of slow dynamics, which does not seem to depend too sensitively on structure formation. This can be understood from the relative insensitivity of the structure to temperature. In the present work, we have varied polydispersity that allows for a large variation of the local structure, and we found that the local structure indeed plays an important role in the development of dynamic correlations and the slow dynamics near glass transition in a supercooled polydisperse liquid. Increasing polydispersity at constant volume fraction leads to a suppression of the rate of growth of dynamic heterogeneity in the system, which can be attributed to the loss of local structure with polydispersity. At moderate polydispersity, there is a faster growth of structural correlations as the temperature is lowered, which leads to a corresponding faster growth of dynamic heterogeneity. At higher polydispersity, structural correlations are weak and do not show any significant change with temperature, and correspondingly, the rate of growth of dynamic correlations is also less. We also find that there is a pronounced local icosahedral order that increases with cooling and decreases with polydispersity. No significant long-range icosahedral order is found either in the equilibrium or supercooled liquid.

An important outcome of the present work is the hitherto unknown correlation between polydispersity and glass forming ability. This correlation deserves further study.

ACKNOWLEDGMENTS

We thank Dr. S. M. Bhattacharryya, Smarajit Karmakar, and Biman Jana for insightful discussions. This work was supported in part by grants from DST, India. S.E.A. acknowledges CSIR, India for support.

[1] G. Adam and J. H. Gibbs, J. Chem. Phys. **43**, 139 (1965).
[2] X. Xia and P. G. Wolynes, Proc. Natl. Acad. Sci. U.S.A. **97**, 2990 (2000); Phys. Rev. Lett. **86**, 5526 (2001).
[3] C. Bennemann, C. Donati, J. Baschnagel, and S. C. Glotzer, Nature **399**, 246 (1999).
[4] L. Berthier, G. Biroli, J.-P. Bouchaud, L. Cipelletti, D. El Marsi, L'Hote, F. Ladieu, and M. Pierno, Science **310**, 1797 (2005).
[5] O. Dauchot, G. Marty, and G. Biroli, Phys. Rev. Lett. **95**, 265701 (2005).
[6] C. Dasgupta, A. V. Indrani, S. Ramaswamy, and M. K. Phani, Europhys. Lett. **15**, 307 (1991).
[7] S. C. Glotzer, V. N. Novikovand, and T. B. Schroder, J. Chem. Phys. **112**, 509 (2000); N. Lacevic, F. W. Starr, T. B. Schroder, and S. C. Glotzer, *ibid.* **119**, 7372 (2003).
[8] E. R. Weeks, J. C. Crocker, A. C. Levitt, A. Schofield, and D. A. Weitz, Science **287**, 627 (2000).
[9] P. Ballesta, A. Duri, and L. Cipelletti, Nat. Phys. **4**, 550 (2008).
[10] R. K. Murarka and B. Bagchi, Phys. Rev. E **67**, 051504 (2003).
[11] S. E. Abraham, S. M. Bhattacharrya, and B. Bagchi, Phys. Rev. Lett. **100**, 167801 (2008).
[12] L. Berthier, G. Biroli, J.-P. Bouchaud, W. Kob, K. Miyazaki, and D. R. Reichman, J. Chem. Phys. **126**, 184503 (2007); **126**, 184504 (2007).
[13] P. J. Steinhardt, D. R. Nelson, and M. Ronchetti, Phys. Rev. B **28**, 784 (1983).
[14] Y. Wang and C. Dellago, J. Phys. Chem. B **107**, 9214 (2003).
[15] Y. Wang, S. Teitel, and C. Dellago, J. Chem. Phys. **122**, 214722 (2005).
[16] C. A. Angell, J. Phys. Chem. Solids **49**, 863 (1988); Science **267**, 1924 (1995).
[17] E. Leutheusser, Phys. Rev. A **29**, 2765 (1984); U. Bengtzelius, W. Gotze, and A. Sjolander, J. Phys. C **17**, 5915 (1984).
[18] S. Bhattacharyya and B. Bagchi, J. Chem. Phys. **106**, 1757 (1997).
[19] F. Ould-Kaddour and J. L. Barrat, Phys. Rev. A **45**, 2308 (1992).
[20] S. Bhattacharyya and B. Bagchi, Phys. Rev. E **61**, 3850 (2000).
[21] G. L. Pollack and J. J. Enyeart, Phys. Rev. A **31**, 980 (1985); G. L. Pollack, R. P. Kennan, J. F. Himm, and D. R. Stump, J. Chem. Phys. **92**, 625 (1990); G. Heuberger and H. Sillescu, J. Phys. Chem. **100**, 15255 (1985).
[22] R. Böhmer, K. L. Ngai, C. A. Angell, and D. J. Plazek, J. Chem. Phys. **99**, 4201 (1993); C. M. Roland and K. L. Ngai, Macromolecules **24**, 5315 (1991); K. Niss, C. Dalle-Ferrier, G. Tarjus, and C. Alba-Simionesco, J. Phys.: Condens. Matter **19**, 076102 (2007).
[23] D. L. Lacks and J. R. Wienhoff, J. Chem. Phys. **111**, 398 (1999).
[24] B. B. Baird and H. R. Schober, Phys. Rev. Lett. **66**, 636 (1991).
[25] A. Heuer and R. J. Silbey, Phys. Rev. Lett. **70**, 3911 (1993).
[26] F. H. Stillinger, Science **267**, 1935 (1995); P. B. Debenedetti and F. H. Stillinger, Nature **410**, 259 (2001);
[27] F. C. Frank, Proc. R. Soc. London, Ser. A **215**, 43 (1952).
[28] T. Egami, in *Rapidly Solidified Alloys*, edited by Howard H. Liberman (CRC, Boca Raton, FL, 1993).
[29] P. Harowell, Conference on Unifying Concepts in Glassy Physics III, Bangalore, 2004.